

Invited talk at the “GAMMA2001” Symposium, April 4-6, 2001, Baltimore.

To be published in “Gamma-Ray Astronomy 2001” (American Institute of Physics)

# Gamma-Ray Signatures of Supernovae and Hypernovae

Ken’ichi Nomoto\*, Keiichi Maeda\*, Yuko Mochizuki<sup>†</sup>, Shiomi Kumagai<sup>\*\*</sup>,  
Hideyuki Umeda\*, Takayoshi Nakamura\* and Isao Tanihata<sup>†</sup>

*\*Department of Astronomy and Research Center for the Early Universe, School of Science,  
University of Tokyo, Bunkyo-ku, Tokyo 113-0033, JAPAN*

*<sup>†</sup>RIKEN (The Institute of Physical and Chemical Research), Hirosawa 2-1, Wako,  
Saitama 351-0198, JAPAN*

*\*\*Department of Physics, College of Science and Technology, Nihon University,  
Kanda-Surugadai 1-8, Chiyoda-ku, Tokyo 101, JAPAN*

## Abstract.

We review the characteristics of nucleosynthesis and radioactivities in ‘Hypernovae’, i.e., supernovae with very large explosion energies ( $\gtrsim 10^{52}$  ergs) and their  $\gamma$ -ray line signatures. We also discuss the  $^{44}\text{Ti}$  line  $\gamma$ -rays from SN1987A and the detectability with INTEGRAL. Signatures of hypernova nucleosynthesis are seen in the large  $[(\text{Ti}, \text{Zn})/\text{Fe}]$  ratios in very metal poor stars. Radioactivities in hypernovae compared to those of ordinary core-collapse supernovae show the following characteristics: 1) The complete Si burning region is more extended, so that the ejected mass of  $^{56}\text{Ni}$  can be much larger. 2) Si-burning takes place in higher entropy and more  $\alpha$ -rich environment. Thus the  $^{44}\text{Ti}$  abundance relative to  $^{56}\text{Ni}$  is much larger. In aspherical explosions,  $^{44}\text{Ti}$  is even more abundant and ejected with velocities as high as  $\sim 15,000 \text{ km s}^{-1}$ , which could be observed in  $\gamma$ -ray line profiles. 3) The abundance of  $^{26}\text{Al}$  is not so sensitive to the explosion energy, while the  $^{60}\text{Fe}$  abundance is enhanced by a factor of  $\sim 3$ .

## INTRODUCTION

Massive stars in the range of 8 to  $\sim 100M_{\odot}$  undergo core-collapse at the end of their evolution and become Type II and Ib/c supernovae (SNe II and SNe Ib/c). These SNe II and SNe Ib/c release large explosion energies and eject explosive nucleosynthesis products, thus being major sources of radioactive species. Until recently, we have considered supernovae with the explosion energies of  $E = 1 - 1.5 \times 10^{51}$  ergs. These energies have been estimated from the observations of nearby supernovae, such as SNe 1987A, 1993J, and 1994I. Also the progenitors of these SNe are estimated to be 13 - 20  $M_{\odot}$  stars (e.g., [1]).

Recently, there have been a number of candidates for the gamma-ray burst (GRB)/supernova (SN) connection (see [1] for references), including GRB980425/SNIc 1998bw, GRB971115/SNIc 1997ef, GRB970514/SNIIn 1997cy, GRB980910/SNIIn 1999E, GRB980326, and GRB970228. Among the SNe with a possible GRB counterpart, SNeIc 1998bw [2, 3] and 1997ef [4, 5] are characterized by a very large kinetic

explosion energy,  $E \gtrsim 10^{52}$  erg. This is more than one order of magnitude larger than in typical SNe, so that these objects may be called "Hypernovae". These SNe produced more  $^{56}\text{Ni}$  than the average core collapse SN. The masses of these hypernova progenitors are estimated to be  $M \gtrsim 25M_{\odot}$ . These massive stars are likely to form black holes, while less massive stars form neutron stars (see, however, [6]).

Regarding  $\gamma$ -ray signatures of such hypernovae, whether and how the hypernovae actually induce gamma-ray bursts needs further study of aspherical explosions (e.g., [7, 8]). Another  $\gamma$ -ray signatures, we discuss here, are the line  $\gamma$ -ray emissions. We review the characteristics of nucleosynthesis and radioactivity in hypernovae and their  $\gamma$ -ray line signatures. We also discuss the  $^{44}\text{Ti}$  line  $\gamma$ -rays from SN1987A and the detectability with INTEGRAL. For line  $\gamma$ -rays from Type Ia supernovae, see Kumagai & Nomoto [9] for a review.

Before discussing  $\gamma$ -rays, we first point out that signatures of hypernova nucleosynthesis are seen in the large  $[(\text{Ti}, \text{Zn})/\text{Fe}]$  ratios in very metal poor stars.

## NUCLEOSYNTHESIS IN HYPERNOVA EXPLOSIONS

In core-collapse supernovae/hypernovae, stellar material undergoes shock heating and subsequent explosive nucleosynthesis. Iron-peak elements are produced in two distinct regions, which are characterized by the peak temperature,  $T_{\text{peak}}$ , of the shocked material. For  $T_{\text{peak}} > 5 \times 10^9 \text{K}$ , material undergoes complete Si burning whose products include Co, Zn, V, and some Cr after radioactive decays. For  $4 \times 10^9 \text{K} < T_{\text{peak}} < 5 \times 10^9 \text{K}$ , incomplete Si burning takes place and its after decay products include Cr and Mn (e.g., [10, 11, 12]).

We note the following characteristics of nucleosynthesis with very large explosion energies [13]:

1) Both complete and incomplete Si-burning regions shift outward in mass compared with normal supernovae, so that the mass ratio between the complete and incomplete Si-burning regions is larger. As a result, higher energy explosions tend to produce larger  $[(\text{Zn}, \text{Co})/\text{Fe}]$ , small  $[(\text{Mn}, \text{Cr})/\text{Fe}]$ , and larger  $[\text{Fe}/\text{O}]$ . The elements synthesized in this region such as  $^{56}\text{Ni}$ ,  $^{59}\text{Cu}$ ,  $^{63}\text{Zn}$ , and  $^{64}\text{Ge}$  (which decay into  $^{56}\text{Co}$ ,  $^{59}\text{Co}$ ,  $^{63}\text{Cu}$ , and  $^{64}\text{Zn}$ , respectively) are ejected more abundantly than in normal supernovae.

2) In the complete Si-burning region of hypernovae, elements produced by  $\alpha$ -rich freezeout are enhanced because nucleosynthesis proceeds at lower densities (i.e., higher entropy) and thus a larger amount of  $^4\text{He}$  is left. Hence, elements synthesized through capturing of  $\alpha$ -particles, such as  $^{44}\text{Ti}$ ,  $^{48}\text{Cr}$ , and  $^{64}\text{Ge}$  (decaying into  $^{44}\text{Ca}$ ,  $^{48}\text{Ti}$ , and  $^{64}\text{Zn}$ , respectively) are more abundant.

3) Oxygen burning takes place in more extended, lower density regions for the larger explosion energy. Hence, O, C, Al are burned more efficiently and their abundances in the ejecta are smaller, while a larger amount of burning products such as Si, S, and Ar are synthesized. Therefore, hypernova nucleosynthesis is characterized by large abundance ratios of  $[\text{Si}/\text{O}]$ ,  $[\text{S}/\text{O}]$ ,  $[\text{Ti}/\text{O}]$ , and  $[\text{Ca}/\text{O}]$ .

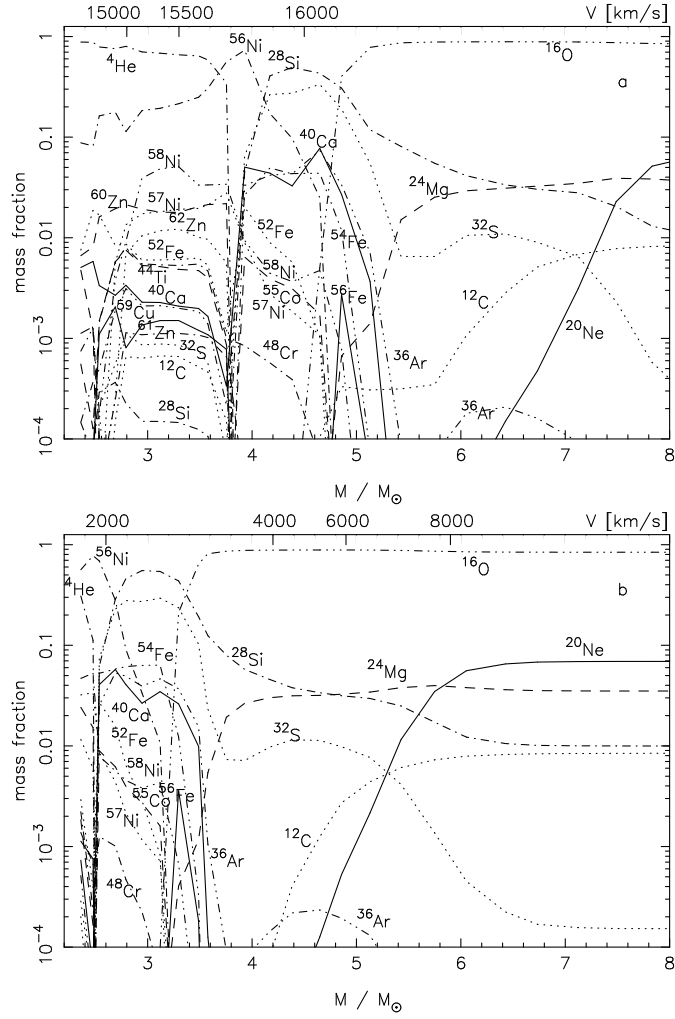


**FIGURE 1.** The isotopic composition of the ejecta in the direction of the jet (upper panel) and perpendicular to it (lower panel). The ordinate indicates the initial spherical Lagrangian coordinate ( $M_r$ ) of the test particles (lower scale), and the final expansion velocities ( $V$ ) of those particles (upper scale) [16].

## ASPHERICAL EXPLOSIONS

Nakamura et al. [14] and Mazzali et al. [15] have identified some signatures of asymmetric explosion in the late light curve and spectra of SN 1998bw. Maeda et al. [16] have examined the effect of aspherical (jet-like) explosions on nucleosynthesis in hypernovae. The progenitor model is the  $16 M_{\odot}$  He core of the  $40 M_{\odot}$  star and the explosion energy is  $E = 1 \times 10^{52}$  ergs.

Figure 1 shows the isotopic composition of the ejecta of asymmetric explosion model in the direction of the jet (upper panel) and perpendicular to it (lower panel).

In the  $z$ -direction, where the ejecta carry more kinetic energy, the shock is stronger and post-shock temperatures are higher. Therefore, larger amounts of  $\alpha$ -rich freeze-out elements, such as  $^4\text{He}$ ,  $^{44}\text{Ti}$ , and  $^{56}\text{Ni}$  are produced in the  $z$ -direction than in the  $r$ -

direction.

On the other hand, along the  $r$ -direction  $^{56}\text{Ni}$  is produced only in the deepest layers, and the elements ejected in this direction are mostly the products of hydrostatic nuclear burning stages (O) with some explosive oxygen-burning products (Si, S, etc).

In the spherical case, Zn is produced only in the deepest layer, while in the aspherical model, the complete silicon burning region is elongated to the  $z$  (jet) direction, so that  $[\text{Zn}/\text{Fe}]$  is enhanced irrespective of the mass cut. On the other hand,  $^{55}\text{Mn}$ , which is produced by incomplete silicon burning, surrounds  $^{56}\text{Fe}$  and located preferentially in the  $r$ -direction.

In this way, larger asphericity in the explosion leads to larger  $[\text{Zn}/\text{Fe}]$  and  $[\text{Co}/\text{Fe}]$ , but to smaller  $[\text{Mn}/\text{Fe}]$  and  $[\text{Cr}/\text{Fe}]$ . Then, if the degree of the asphericity tends to be larger for lower  $[\text{Fe}/\text{H}]$ , the trends of  $[(\text{Zn}, \text{Co}, \text{Mn}, \text{Cr})/\text{Fe}]$  follow the ones observed in metal-poor stars, as discussed later.

## SIGNATURES OF HYPERNOVA NUCLEOSYNTHESIS IN GALACTIC CHEMICAL EVOLUTION

Several observational signatures of hypernova nucleosynthesis have been noticed in several objects [13]. The abundance pattern of metal-poor stars with  $[\text{Fe}/\text{H}] < -2$  provides us with very important information on the formation, evolution, and explosions of massive stars in the early evolution of the galaxy.

In the early galactic epoch when the galaxy is not yet chemically well-mixed,  $[\text{Fe}/\text{H}]$  may well be determined by mostly a single SN event [18]. The formation of metal-poor stars is supposed to be driven by a supernova shock, so that  $[\text{Fe}/\text{H}]$  is determined by the ejected Fe mass and the amount of circumstellar hydrogen swept-up by the shock wave [19]. Then, hypernovae with larger  $E$  are likely to induce the formation of stars with smaller  $[\text{Fe}/\text{H}]$ , because the mass of interstellar hydrogen swept up by a hypernova is roughly proportional to  $E$  [19, 20] and the ratio of the ejected iron mass to  $E$  is smaller for hypernovae than for canonical supernovae.

The observed abundances of metal-poor halo stars show quite interesting pattern. There are significant differences between the abundance patterns in the iron-peak elements below and above  $[\text{Fe}/\text{H}] \sim -2.5$  -  $-3$ , which cannot be explained with the conventional chemical evolution model that uses previous nucleosynthesis yields.

1) For  $[\text{Fe}/\text{H}] \lesssim -2.5$ , the mean values of  $[\text{Cr}/\text{Fe}]$  and  $[\text{Mn}/\text{Fe}]$  decrease toward smaller metallicity, while  $[\text{Co}/\text{Fe}]$  increases [21, 19].

2)  $[\text{Zn}/\text{Fe}] \sim 0$  for  $[\text{Fe}/\text{H}] \simeq -3$  to  $0$  [22], while at  $[\text{Fe}/\text{H}] < -3.3$ ,  $[\text{Zn}/\text{Fe}]$  increases toward smaller metallicity [23, 24].

The larger  $[(\text{Zn}, \text{Co})/\text{Fe}]$  and smaller  $[(\text{Mn}, \text{Cr})/\text{Fe}]$  in the supernova ejecta can be realized if the mass ratio between the complete Si burning region and the incomplete Si burning region is larger, or equivalently if deep material from complete Si-burning region is ejected by mixing or aspherical effects. This can be realized if (1) the mass cut between the ejecta and the collapsed star is located at smaller  $M_r$  [26], (2)  $E$  is larger to move the outer edge of the complete Si burning region to larger  $M_r$  [27], or (3) asphericity in the explosion is larger.

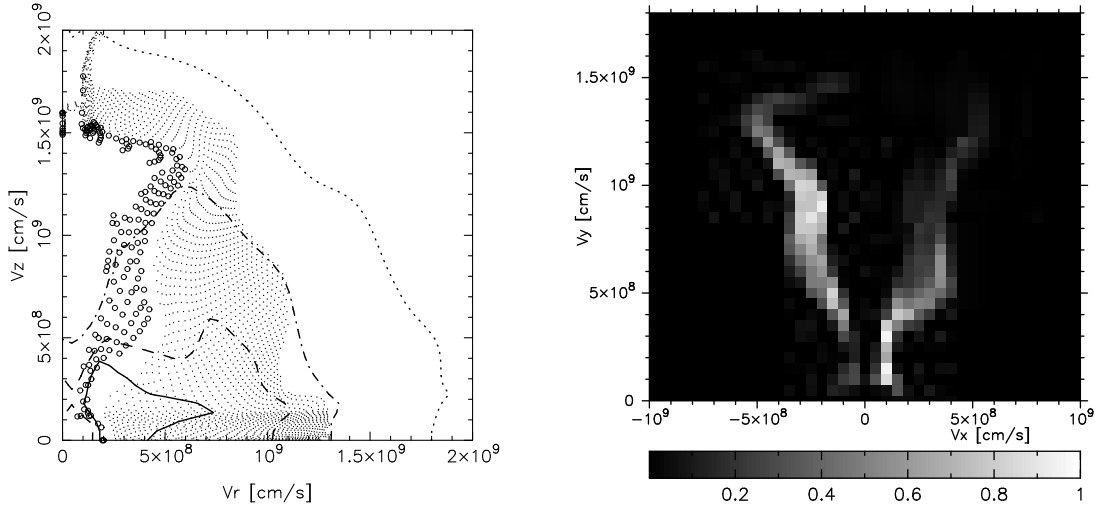


**FIGURE 2.** Left: The distribution of  $^{56}\text{Ni}$  (open circles) and  $^{16}\text{O}$  (dots) with density contours (lines) [16]. Right: The density distributions of  $^{44}\text{Ti}$  (left half) and  $^{56}\text{Ni}$  (right half). The densities of each element are represented with linear scale, from 0 to the max density of each element [28].

Also a large explosion energy  $E$  results in the enhancement of the local mass fractions of Zn and Co, while Cr and Mn are not enhanced [25]. Models with  $E_{51} = E/10^{51}$  ergs do not produce sufficiently large  $[\text{Zn}/\text{Fe}]$ . To be compatible with the observations of  $[\text{Zn}/\text{Fe}] \sim 0.5$ , the explosion energy must be much larger, i.e.,  $E_{51} \gtrsim 20$  for  $M \gtrsim 20M_{\odot}$ .

Therefore, if hypernovae made significant contributions to the early Galactic chemical evolution, it could explain the large Zn and Co abundances and the small Mn and Cr abundances observed in very metal-poor stars.

## NUCLEAR RADIOACTIVITY IN HYPERNOVAE

Hypernovae produce radioactive species in larger amount than normal SNe II, thus being important sources of line  $\gamma$ -rays and positrons.

### $^{56}\text{Ni}$ and Positrons

A large amount of  $^{56}\text{Ni}$  can be produced as actually observed:  $\sim 0.5 M_{\odot}$  from SN1998bw,  $\sim 0.15M_{\odot}$  from SN1997ef, and even much larger from SN1999as. Thus hypernovae are the important source of positrons as well. In particular, positrons in the galactic center region might be significantly contributed by hypernovae, because as observed in M82 [13], hypernovae would make an important contribution in nucleosynthesis associated with starburst events.

**TABLE 1.** The mass ratio  $^{44}\text{Ti}/^{56}\text{Ni}$  for  $40M_{\odot}$  models [28]. Values of spherical models are taken from Nakamura et al. [27].

Spherical ( $E_{51} = 1$ )	Spherical ( $E_{51} = 10$ )	Aspherical ( $E_{51} = 10$ )
6.51E-4	2.79E-3	1.01E-2

**TABLE 2.** Mass of  $^{26}\text{Al}$  and  $^{60}\text{Fe}$  ( $M_{\odot}$ ) ( $Z=0.02$ ) [25].

$E_{51}$	1	10	1	10
$M$	$^{26}\text{Al}$		$^{60}\text{Fe}$	
$20M_{\odot}$	8.87e-5	5.73e-5	1.37E-5	1.31E-4
$25M_{\odot}$	1.17e-4	1.22e-4	1.86E-4	3.38E-4
$40M_{\odot}$	8.61e-5	1.20e-4	1.82E-5	2.47E-5

## $^{44}\text{Ti}$

$^{44}\text{Ti}$  is synthesized in the  $\alpha$ -rich freezeout, in complete Si burning. In the very high entropy environment in hypernovae, the photons dissociate all the preexisting nuclei down to essentially  $\alpha$ -particles and neutrons. The abundances then shift to those in nuclear statistical equilibrium but freezes out with excess  $\alpha$ -particles. The  $^{44}\text{Ti}$  yield depends strongly on the location of the mass cut, electron fraction, and entropy condition in the  $\alpha$ -rich freezeout. Therefore the initial yield of  $^{44}\text{Ti}$  provides unique information to constrain the explosion models.

Iron-peak elements are produced in the deep region near the mass cut, so that their production is strongly affected by asphericity of an explosion. Figure 2 shows the 2D density distribution of  $^{44}\text{Ti}$  and  $^{56}\text{Ni}$ , which is distributed preferentially in the  $z$ -direction.  $^{44}\text{Ti}$ , which is produced by the strong  $\alpha$ -rich freezeout, is distributed preferentially in the  $z$ -direction. Moreover,  $^{44}\text{Ti}$  production is strongly enhanced compared with a spherical model [28, 29], since the post-shock temperature along the  $z$ -direction is much higher than that of a spherical model.

Table 1 summarize the mass ratio  $^{44}\text{Ti}/^{56}\text{Ni}$  produced in the spherical and the aspherical explosion of the  $40 M_{\odot}$  models. We can see that  $^{44}\text{Ti}$  is strongly enhanced in hypernova and aspherical models [28]. The  $\gamma$ -rays from the decays of  $^{44}\text{Ti}$  are possible tools to investigate the Galactic hypernova remnants.

## $^{26}\text{Al}$ and $^{60}\text{Fe}$

Preliminary results of  $^{26}\text{Al}$  and  $^{60}\text{Fe}$  are summarized in Table 2 [25].

- 1) The  $^{26}\text{Al}$  abundance does not depend much on  $E$ . It is a little smaller in hypernovae than supernovae, because more  $^{26}\text{Al}$  is consumed in oxygen burning as are O, Mg, Ne.
- 2)  $^{60}\text{Fe}$  abundance is larger by a factor of  $\sim 1.5 - 10$ .

## RX J0852-4622/GRO J0854-4622

COMPTEL has detected the  $^{44}\text{Ti}$  1157 keV  $\gamma$ -ray line from the supernova remnant (SNR) RX J0852-4622 [30, 31, 32], though the evidence is found at the  $2\sigma$  to  $4\sigma$  significance level [33]. ASCA has observed RX J0852-4622 and detected the 4.1 keV X-ray emission line from Ca [34]. Tsunemi et al. [34] have provided the following analysis and interpretation. The abundance of Ca is oversolar by a factor of  $8 \pm 5$ , while other elements are subsolar. The mass of Ca is  $\sim 1.1 \times 10^{-3} M_{\odot}$ . The excess Ca is likely to be  $^{44}\text{Ca}$ , the decay product of  $^{44}\text{Ti}$ . This feature is seen only in the north-west shell, which suggests that the supernova ejecta has just collided with the interstellar material there.

Iyudin & Aschenbach [35] have assumed that the width of the  $^{44}\text{Ti}$  line is due to Doppler broadening and thus  $^{44}\text{Ti}$  is expanding at  $\sim 15,000 \text{ km s}^{-1}$  [30]. Then they suggested that such high velocity  $^{44}\text{Ti}$  is ejected from a Type Ia supernova of sub-Chandrasekhar mass [36, 37], because the model produces  $\sim 10^{-3} M_{\odot}$   $^{44}\text{Ti}$  in the outer He detonation zone which expands at  $\sim 15,000 \text{ km s}^{-1}$ .

Here we suggest an alternative model for the high velocity  $^{44}\text{Ti}$ . As seen in Figure 2, the asymmetric hypernova explosion ejects  $^{44}\text{Ti}$  at  $\sim 15,000 \text{ km s}^{-1}$  in the jet direction. The amount of  $^{44}\text{Ti}$  is as large as  $1 \times 10^{-3} M_{\odot}$  (Table 1), being consistent with the observation.

INTEGRAL observations of the  $^{44}\text{Ti}$  lines and their line profiles from RX J0852-4622 are important to discriminate the models and clarify the energetics of the explosion.

## SN 1987A

SN 1987A in the LMC has shown for the first time that the energy source of supernova ejecta directly comes from the decays of radioactive nuclei (e.g., [38, 39]) for reviews). In this section, we investigate the initial abundance of  $^{44}\text{Ti}$  to discuss the detection possibility of the line gamma-rays from SN 1987A, by comparing theoretical light curves with the observed bolometric luminosity of SN 1987A.

In SN 1987A, it is established that the observed light curve in early time is first governed by  $^{56}\text{Ni}$  [ $t_{1/2}$  (half-life) = 6.1 d] and then its daughter  $^{56}\text{Co}$  ( $t_{1/2} = 77.3 \text{ d}$ ). The synthesized  $^{56}\text{Co}$  nuclide decays to stable  $^{56}\text{Fe}$ . As we shall see later, the observed light curve in the wavelength ranging from ultraviolet (UV) to infrared (IR) has been successfully modeled with the energy supply from the decay of  $^{56}\text{Co}$  until  $\sim 800$  days (e.g., [38]). This has been directly confirmed by the detection of the hard X-rays and the line  $\gamma$ -rays from the decay sequence of  $^{56}\text{Co}$ .

Afterwards, the decline of the observed light curve apparently slowed down, due to the decay of  $^{57}\text{Co}$  ( $t_{1/2} = 272 \text{ d}$ ). The slowness of the decline of observed light curve becomes distinguished in particular after  $\sim 1500$  days from the explosion. The dominant energy source at this moment can be attributed to  $^{44}\text{Ti}$  decay.  $^{44}\text{Ti}$  decays by orbital electron capture to  $^{44}\text{Sc}$ , emitting 67.9 keV (100 %) and 78.4 keV (98 %) lines.  $^{44}\text{Sc}$  then decays mainly by positron emission into  $^{44}\text{Ca}$ , which emits a 1157 keV (100 %) de-excitation line.

Obviously, a luminosity observation in SN 1987A of late years is crucial to study the

property of the extra energy source, namely, the  $^{44}\text{Ti}$  production. Recently, this crucial luminosity at 3600 days, i.e., 10 years after the explosion was reported by Suntzeff [40]. The observed luminosity in the UV-IR range is  $L = (1.9 \pm 0.6) \times 10^{36} \text{ erg sec}^{-1}$ . The result is obtained by the collaboration of CTIO with HST, and hereafter we refer to this as the CTIO+HST luminosity. In the following, we investigate whether the  $^{44}\text{Ti}$  decay provides enough energy to account for the observed CTIO+HST luminosity under the latest half-life value of  $^{44}\text{Ti}$  [41].

## The Half-Life of $^{44}\text{Ti}$

The energy release from the  $^{44}\text{Ti}$  decay depends strongly on its half-life. With recent experimental efforts, the half-life appears to be settled in  $60 \pm 3$  years, including the errors up to  $3 \sigma$  (see [42] and references therein).

We note here that the half-life values obtained in laboratories are for neutral atoms. Since  $^{44}\text{Ti}$  undergoes pure orbital electron capture decay, its decay rate becomes smaller than the experimental value if  $^{44}\text{Ti}$  is highly ionized under the condition of a supernova. For example, the decay rates of hydrogen-like and helium-like ions are, respectively,  $\sim 44 \%$  and  $\sim 88 \%$  of those of neutral atoms. Details are found in Mochizuki et al. [43] and Mochizuki [44].

It is expected that  $^{44}\text{Ti}$  was neutral when the CTIO+HST observation was carried out. We thus adopt  $60 \pm 3$  years to calculate theoretical light curves to compare the observation.

## Theoretical Light Curve of SN 1987A

Our calculation of the light curves is based on Kumagai et al. [38] and the adopted nuclear decay property data are updated. We perform Monte Carlo simulations of the Compton degradation of the line  $\gamma$ -rays emitted from the decays of  $^{57}\text{Co}$  (14 keV, 122 keV, 136 keV, etc.) and  $^{44}\text{Ti}$  (68 keV, 78 keV, 1157 keV) to obtain the UV-IR light curves. The UV, optical, and IR photons originate from the energy loss of the emitted  $\gamma$ -rays during the radiative transfer in the ejecta. The calculated UV-IR luminosity is the result of subtracting the energy of the X-ray and  $\gamma$ -ray photons which have managed to get out of the remnant.

For the velocity distribution of particles, we adopt the explosion model 14E1 proposed by Shigeyama & Nomoto [45] whose main-sequence mass, ejecta mass, and explosion energy are  $20 M_{\odot}$ ,  $14.6 M_{\odot}$  ( $4.4 M_{\odot}$  core material plus  $10.2 M_{\odot}$  hydrogen-rich envelope), and  $1 \times 10^{51}$  erg, respectively. This model was derived from a detailed analysis of the plateau shape of the light curve of SN 1987A which is observed until 120 days after the explosion, and well accounts for the earlier optical, X-ray, and  $\gamma$ -ray light curves of SN 1987A [46]. Note that the  $^{56}\text{Ni}$  mass in SN 1987A has been constrained as  $0.07 M_{\odot}$  from the intensity during the observed exponential decline. The synthesized mass of the radioactive  $^{57}\text{Ni}$  is adopted from Hashimoto, Nomoto, & Shigeyama [10], and the input value of the initial  $^{44}\text{Ti}$  abundance is varied within the uncertainty studied in Hashimoto



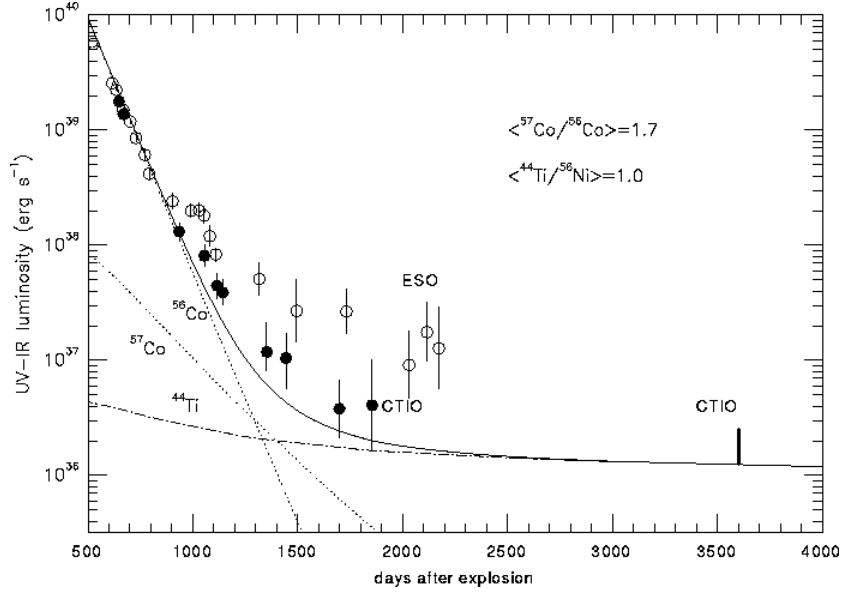


**FIGURE 3.** The calculated light curve and the observed bolometric (UV to IR) luminosity of SN 1987A, including the latest observed luminosity (CTIO+HST).

et al. [10] to compare the CTIO+HST luminosity.

In Figure 3, we show the calculated UV-IR light curve (solid) and the observed luminosities of SN1987A (CTIO and ESO). For this, the  $^{44}\text{Ti}$  half-life of 60 yrs and  $\langle^{44}\text{Ti}/^{56}\text{Ni}\rangle = 1$  have been adopted. Here,  $\langle^{44}\text{Ti}/^{56}\text{Ni}\rangle$  is defined as the ratio of  $^{44}\text{Ti}/^{56}\text{Ni}$  in SN1987A to  $^{44}\text{Ca}/^{56}\text{Fe}$  in the solar neighborhood, i.e.,  $\langle^{44}\text{Ti}/^{56}\text{Ni}\rangle \equiv [X(^{44}\text{Ti})/X(^{56}\text{Ni})]/[X(^{44}\text{Ca})/X(^{56}\text{Fe})]_{\odot}$ . The three decay sequences of  $^{56}\text{Ni}$ ,  $^{57}\text{Ni}$  and  $^{44}\text{Ti}$  are used for the energy sources as shown in Figure 3. We found that the observed CTIO+HST luminosity is reasonably explained with the energy release from the  $^{44}\text{Ti}$  decay for its half-life of  $60 \pm 3$  yrs.

### Production of $^{44}\text{Ti}$ in SN 1987A

The  $\langle^{44}\text{Ti}/^{56}\text{Ni}\rangle$  values that are required to explain the CTIO+HST luminosity are found to be roughly between 1 and 2. Since the synthesized mass of  $^{56}\text{Ni}$  has been determined to be  $0.07M_{\odot}$  for SN 1987A, the obtained  $\langle^{44}\text{Ti}/^{56}\text{Ni}\rangle$  values can directly be translated to the initial mass of  $^{44}\text{Ti}$ . Note that the amount of  $^{44}\text{Ti}$  is the total value that is responsible for the overall energy in  $\gamma$ -rays, X-rays, and in the UV-IR range.

We thus obtained that the initial  $^{44}\text{Ti}$  mass is  $(1.1 - 2.5) \times 10^{-4} M_{\odot}$  for the half-life value of  $60 \pm 3$  yrs. We remark that the  $^{44}\text{Ti}$  yield calculated from recent explosive nucleosynthesis models overlap with our estimate (e.g., [47, 48, 49]). However, it should be also mentioned that these model predictions are subject to nuclear reaction cross sections which have not yet measured so far (see, [50, 51]).

Note that Chugai et al. [52] estimated that positrons from  $(1-2) \times 10^{-4} M_{\odot}$  of  $^{44}\text{Ti}$  provides the overall luminosity of the FeII emission lines, and Lundqvist et al. [53, 54]

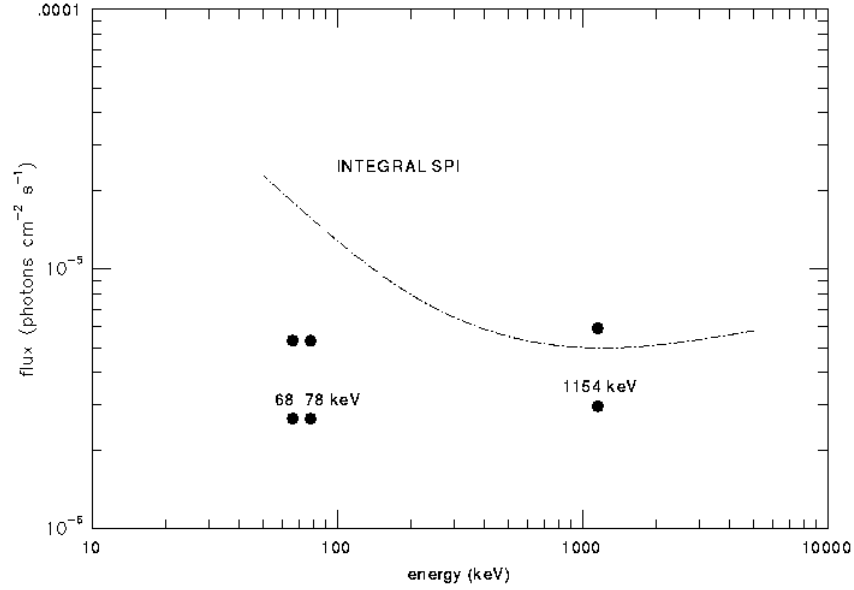


**FIGURE 4.** Predictions of the line gamma-ray fluxes from the  $^{44}\text{Ti}$  decay sequence (filled circles) for the initial mass of  $^{44}\text{Ti}$  of  $1 \times 10^{-4} M_{\odot}$  and  $2 \times 10^{-4} M_{\odot}$ , respectively. The sensitivity limit of INTEGRAL SPI ( $10^6$  sec) is also shown by the dash-dotted curve.

obtained the upper limit of the  $^{44}\text{Ti}$  mass,  $1 - 1.5 \times 10^{-4} M_{\odot}$ , based on ISO SWS/LWS observations.

### $^{44}\text{Ti}$ in SN 1987A with INTEGRAL

Detection of  $^{44}\text{Ti}$  line  $\gamma$ -rays from SN 1987A should be an important target for the INTEGRAL mission. In Figure 4, we show the expected fluxes from SN 1987A on Earth for 68, 78, and 1157 keV lines, respectively. For each  $\gamma$ -ray line in Figure 4, the upper and lower filled circles are calculated for the  $^{44}\text{Ti}$  yield of  $2 \times 10^{-4} M_{\odot}$ , and  $1 \times 10^{-4} M_{\odot}$ , respectively. In Figure 4, the sensitivity limit of INTEGRAL SPI ( $10^6$  sec) is also shown, which strongly depends on energy. We see from Figure 4 that it is possible to marginally detect the 1157 keV line if the produced amount of  $^{44}\text{Ti}$  is as large as  $2 \times 10^{-4} M_{\odot}$ , but for other cases the expected fluxes lie below the sensitivity limit of SPI.

In the above discussion of the expected fluxes, no ionization effect on the  $^{44}\text{Ti}$  decay is taken into account. Recently, helium-like and hydrogen-like ions of O, Ne, Mg, and Si have been observed with Chandra X-ray observatory [55]. The ionization of the ejected material was caused by the shock heating associated with the collision with the circumstellar matter (including the ring). As discussed previously, the decay rate of highly ionized  $^{44}\text{Ti}$  can become considerably small compared with that of neutral  $^{44}\text{Ti}$ . This means, as claimed by Mochizuki [44], all the  $^{44}\text{Ti}$   $\gamma$ -ray line fluxes from SN 1987A possibly lie below the detection limit of INTEGRAL SPI.

Finally, we should note that INTEGRAL has capabilities both in the detection of nuclear lines and pulsed emission. It has not been clear yet whether SN1987A has

formed a neutron star or a black hole. It is certainly worth trying for INTEGRAL and Astro E-II to search for pulsation.

## ACKNOWLEDGMENTS

This work has been supported in part by the grant-in-Aid for Scientific Research (07CE2002, 12640233) of the Ministry of Education, Science, Culture, and Sports in Japan.

## REFERENCES

1. Nomoto, K., et al. 2001, in “Supernovae and Gamma Ray Bursts” eds. M. Livio, et al. (Cambridge Univ. Press), 144 (astro-ph/0003077)
2. Iwamoto, K., Mazzali, P.A., Nomoto, K., et al. 1998, *Nature*, 395, 672
3. Woosley, S.E., Eastman, R.G., & Schmidt, B.P. 1999, *ApJ*, 516, 788
4. Iwamoto, K., Nakamura, T., Nomoto, K., et al. 2000, *ApJ*, 534, 660
5. Mazzali, P.A., Iwamoto, K., & Nomoto, K. 2000, *ApJ*, 545, 407
6. Wheeler, J. C., Yi, I., Höflich, P. A., & Wang, L. 2000, *ApJ*, 537, 810
7. MacFadyen, A.I. & Woosley, S.E. 1999, *ApJ* 524, 262
8. Khokhlov, A.M., Höflich, P.A., Oran, E.S., Wheeler, J.C., Wang, L., & Chtchelkanova, A.Yu. 1999, *ApJ*, 524, L107
9. Kumagai, S., & Nomoto, K. 1997, in *Thermonuclear Supernovae*, ed. P. Ruiz-Lapuente, et al. (Kluwer), 515
10. Hashimoto, M., Nomoto, K., & Shigeyama, T. 1989, *A&A*, 210, L5
11. Woosley, S. E., & Weaver, T. A. 1995, *ApJS*, 101, 181
12. Thielemann, F.-K., Nomoto, K., & Hashimoto, M. 1996, *ApJ*, 460, 408
13. Nomoto, K., Maeda, K., Umeda, H., & Nakamura, T. 2001, in *The Influence of Binaries on Stellar Populations Studies*, ed. D. Vanbeveren (Kluwer), 507 (astro-ph/0105127)
14. Nakamura, T., Mazzali, P. A., Nomoto, K., & Iwamoto, K. 2001a, *ApJ*, 550, 991
15. Mazzali, P.A., Nomoto, K., Patat, F., & Maeda, K. 2001, *ApJ*, in press (astro-ph/0106095)
16. Maeda, K., Nakamura, T., Nomoto, K., Mazzali, P.A., & Hachisu, I. 2002, *ApJ*, 565, in press (astro-ph/0011003)
17. Patat, F., et al. 2001, *ApJ*, 555, 900
18. Audouze, J., & Silk, J. 1995, *ApJ*, 451, L49
19. Ryan, S.G., Norris, J.E. & Beers, T.C. 1996, *ApJ*, 471, 254
20. Shigeyama, T., & Tsujimoto, T. 1998, *ApJ*, 507, L135
21. McWilliam, A., Preston, G.W., Sneden, C., & Searle, L. 1995, *AJ*, 109, 2757
22. Sneden, C., Gratton, R.G., & Crocker, D.A. 1991, *A&A*, 246, 354
23. Primas, F., Reimers, D., Wisotzki, L., Reetz, J., Gehren, T., & Beers, T.C. 2000, in *The First Stars*, ed. A. Weiss, et al. (Springer), 51
24. Blake, L.A.J., Ryan, S.G., Norris, J.E., & Beers, T.C. 2001, *Nucl.Phys.A*.
25. Umeda, H., & Nomoto, K. 2001, *ApJ*, 563, in press (astro-ph/0103241)
26. Nakamura, T., Umeda, H., Nomoto, K., Thielemann, F.-K., & Burrows, A. 1999, *ApJ*, 517, 193
27. Nakamura, T., Umeda, H., Iwamoto, K., Nomoto, K., Hashimoto, M., Hix, R.W., Thielemann, F.-K. 2001b, *ApJ*, 555, 880
28. Maeda, K. 2001, Master Thesis, University of Tokyo
29. Nagataki, S., Hashimoto, M., Sato, K., Yamada, S. 1997, *ApJ*, 486, 1026
30. Iyudin, A.F., Schönfelder, V., Bennett, K., et al. 1998, *Nature*, 396, 142
31. Aschenbach, B. 1998, *Nature*, 396, 141
32. Aschenbach, B., Iyudin, A.F., & Schönfelder, V. 1999, *A&A*, 350, 997
33. Schönfelder, V., Bloemen, H., Collmar, W., Diehl, R., et al. 2000, 5th Compton Symp., AIP, 510, 54

34. Tsunemi, H., Miyata, E., Aschenbach, B., Hiraga, J., & Akutsu, D. 2000, PASJ, 52, 887
35. Iyudin, A.F., & Aschenbach, B. 2001, in *New Century of X-ray Astronomy*, ed. H. Kunieda (AIP)
36. Livne, E., & Arnett, D. 1995, ApJ, 452, L62
37. Arnett, W. D., *Supernovae and Nucleosynthesis* (Princeton Univ. Press)
38. Kumagai, S., Nomoto, K., Shigeyama, T., Hashimoto, M., & Itoh, M. 1993, A&A, 273, 153
39. Nomoto, K., et al. 1994, in *Supernovae (Les Houches, Session LIV)* ed. S. Bludman et al. (Elsevier Science Pub.), 199
40. Suntzeff, N.B. 1997, in *SN1987A: Ten Years After*, eds. M.M. Phillips and N.B. Suntzeff (PASP).
41. Mochizuki, Y.S., Kumagai, S., Tanihata, I. 1998, in *Origin of Matter and Evolution of Galaxies*, eds. S. Kubono et al. (World Scientific), 327
42. Hashimoto, T., Nakai, K., Wakasaya, Y., et al. 2001, Nucl. Phys. A686, 591
43. Mochizuki, Y., Takahashi, K., Janka, H.-Th., Hillebrandt, W., & Diehl, R. 1999, A&A, 346, 831
44. Mochizuki, Y. 2001, Nucl. Phys. A688, 58c
45. Shigeyama, T. & Nomoto, K. 1990, ApJ, 360, 242
46. Nomoto, K., Shigeyama, T., Kumagai, S., Yamaoka, H. 1991, in *Supernovae*, ed. S.E. Woosley (Springer), 176
47. Thielemann, F.-K., Hashimoto, M., & Nomoto, K. 1990, ApJ, 349, 222
48. Timmes, F.X., Woosley, S.E., Hartmann, D.H., & Hoffman, R.D. 1996, ApJ, 464, 332
49. Woosley, S.E. & Hoffman, R.D. 1991, ApJ, 368, L31
50. The, L.-S., Clayton, D.D., Jin, L., & Meyer, B.S. 1998, ApJ, 504, 500
51. Sonzogni, A.A., Rehm, K.E., Ahmad, I., et al. 2000, Phys. Rev. Lett. 84, 1651
52. Chugai, N.N. et al. 1997, ApJ, 483, 925
53. Lundqvist, P., Sollerman, J., Kozma, C. et al. 1999, A&A, 347, 500
54. Lundqvist, P., Kozma, C., Sollerman, J., & Fransson, C. 2001, A&A, 374, 629
55. Burrows, D.N., Michael, E., Hwang, U., et al. 2000, ApJ, 543, L149